Volume 9
Number 25
7 July 2021
Pages 14105–14610

Journal of Materials Chemistry A

Materials for energy and sustainability

rsc.li/materials-a

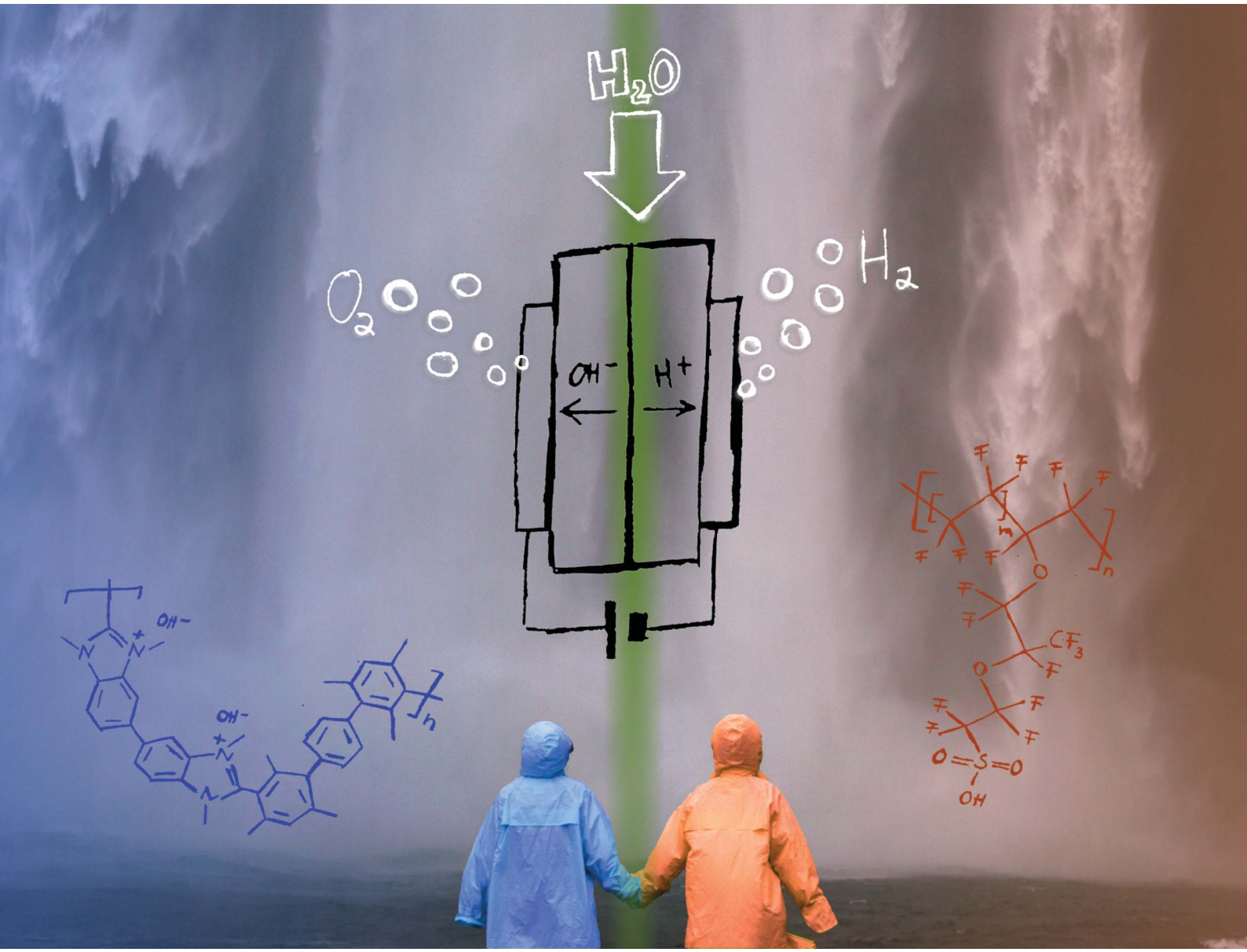

ISSN 2050-7488

ROYAL SOCIETY OF CHEMISTRY

PAPER

Simon Thiele *et al.*

On the effect of anion exchange ionomer binders in bipolar electrode membrane interface water electrolysis

Journal of Materials Chemistry A

ROYAL SOCIETY OF CHEMISTRY

PAPER

View Article Online
View Journal | View Issue

Cite this: J. Mater. Chem. A, 2021, 9, 14285

On the effect of anion exchange ionomer binders in bipolar electrode membrane interface water electrolysis†

Britta Mayerhöfer, [ab] Konrad Ehelebe, [ab] Florian D. Speck, [ab] Markus Bierling, [ab] Johannes Bender, [c] Jochen A. Kerres, [acd] Karl J. J. Mayrhofer, [ab] Serhiy Cherevko, [a] Retha Peach [a] and Simon Thiele *[ab]

Bipolar membrane|electrode interface water electrolyzers (BPEMWE) were found to outperform a proton exchange membrane (PEM) water electrolyzer reference in a similar membrane electrode assembly (MEA) design based on individual porous transport electrodes (PTE) and a free-standing membrane. We present a detailed study on bipolar interfaces between anion exchange ionomer (AEI) based anode catalyst layers in direct contact with a PEM aiming to unravel influences of local pH, the water splitting bipolar interface and catalyst layer structure. It is conventionally accepted that AEIs used in anion exchange- and bipolar membrane water electrolysis conduct hydroxide anions and ensure a high pH environment in the catalyst layer. We have investigated the effect of different ionomers on the local pH at a metal surface and found a strong correlation with the pH of the surrounding solution rather than the ionomer type. Thus, solely the use of an AEI cannot maintain high pH. A study on BPEMWEs revealed strong indications for the co-existence of a water dissociating bipolar interface, and an acidic oxygen evolution mechanism. The superior performance compared to a PTE-based PEM water electrolyzer seems to stem from reduced contact resistances due to adhesive effects between the oppositely charged polymers. Our study shows that the bipolar approach can be utilized to make PTE-based electrolyzers competitive to commonly employed catalyst coated membranes.

Received 26th January 2021
Accepted 14th May 2021

DOI: 10.1039/d1ta00747e

rsc.li/materials-a

Introduction

Electrochemical hydrogen production is considered an essential cornerstone for establishing a future energy economy without fossil fuels. Even though there are many advances in all technological directions of water electrolysis, more than 96% [1] of the hydrogen produced today still originates from carbon-based energy carriers, which stresses the need for further cost optimization of this energy storage vector.[2,3]

Besides mature alkaline- (AWE)[4] and proton exchange membrane water electrolysis (PEMWE),[5] the relatively uncharted field of anion exchange membrane water electrolysis (AEMWE, Fig. 1a) is gaining more and more interest. AEMWE is considered a possible strategy to implement zero-gap membrane electrode assemblies allowing for high gas purity, conceivable pressure operation just like PEMWE but with the advantage of the possible implementation of low-cost catalyst materials and bipolar plates as featured in AWE.[6] As hydroxide conducting anion exchange polymers are used as membranes and ionomers in catalyst layers, it is widely anticipated that an alkaline environment surrounds the catalytic sites. Therefore, low-cost platinum group metal (PGM) free catalysts are expected to be stable, even in the case of a pure water feed into the membrane electrode assembly (MEA).[7–10] Another very recent approach emerging based on higher technological readiness levels of AEM materials are bipolar membrane water electrolyzers (BPMWE), theoretically allowing optimal pH conditions at the individual electrodes.[11]

There are quite a few examples in the literature on membrane-based energy conversion devices (*e.g.*, fuel cells or CO_2-electrolyzers and solar-driven water splitting[12]), which utilize the advantages of bipolar membranes. In CO_2 electrolysis, bipolar membranes act as functional separators to prevent bicarbonate crossover, and the electrolyte solutions establish the electrode pH.[13–16] For fuel cells, mainly water recombination

[a]Forschungszentrum Jülich GmbH, Helmholtz-Institute Erlangen-Nürnberg for Renewable Energy (IEK-11), Cauerstr. 1, 91058 Erlangen, Germany. E-mail: si.thiele@fz-juelich.de

[b]Friedrich-Alexander University Erlangen-Nürnberg, Department for Chemical and Biological Engineering, Egerlandstr. 3, 91058 Erlangen, Germany

[c]University of Stuttgart, Institute of Chemical Process Engineering (ICVT), Boeblinger Str. 78, 70199 Stuttgart, Germany

[d]Focus Area: Chemical Resource Beneficiation Faculty of Natural Sciences, North-West University, Potchefstroom 2520, South Africa

† Electronic supplementary information (ESI) available. See DOI: 10.1039/d1ta00747e

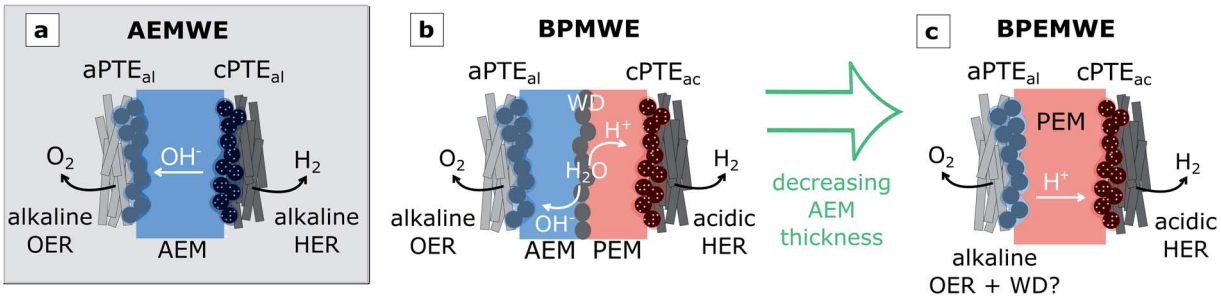

Fig. 1 Schematic representation of (a) an AEMWE-, and (b) a BPMWE MEA with solid AEM and PEM water dissociation (WD) catalyst layer at the AEM|PEM interface. Decrease of AEM layer thickness down to the limiting case of (c) a bipolar membrane|electrode water electrolyzer (BPEMWE).[24]

at the bipolar interface is implemented by an alkaline cathode and an acidic anode. This configuration enables the self-humidification of the fuel cell. Further, it has been shown that the best cell performance is achieved with the bipolar interface directly positioned between the anion exchange ionomer (AEI, here always denoted as electrode binder) based cathode electrode and the PEM.[17] The existence of an actual pH gradient caused only by the combination of an AEM and a PEM was experimentally investigated for direct borohydride fuel cells. Recessed planar electrode measurements and electron microscopy were employed to study a drastic change in the reaction mechanism with the respective electrodes' changing pH environment.[18] Furthermore, PGM-free cathode catalysts showed lower voltage loss during constant current operation in a bipolar approach compared to a PEM reference. However, water management remains an unsolved problem hindering high current density operation.[19]

In water electrolysis, the opposite configuration is considered more advantageous: An AEM for the anode side is expected to enable the use of low-cost oxygen evolution (OER) catalysts. In contrast, the cathode side is kept in a PEM environment as the hydrogen evolution reaction (HER) requires only very low amounts of Pt catalyst and is favorable in acidic media.[20,21] The additionally created bipolar interface drives water dissociation into protons and hydroxide (Fig. 1b), which feed the respective electrode reactions.[22–24] Interested readers are referred to a recent review by Giesbrecht *et al.*[25]

There are opposing opinions in the literature on how a stable pH gradient needs to be implemented in a real water electrolysis device. In contrast to fuel cells, water electrolyzers feature membrane and AEI soaked in a liquid electrolyte. Thus the IUPAC definition of pH as hydrogen ion (proton) activity in (aqueous) solution[26] is more comprehensible under these high humidification levels of membrane and ionomer binders. However, it is unclear to what extent the ionomer and the surrounding solution (including electrode reactions) influence the local pH in the MEA. Some reports propose the necessity to combine a feed of liquid acid and base to establish low and high pH at anode and cathode, respectively, combined with a bipolar membrane for water splitting.[27] However, co- and counter-ion leakage through the membrane driven by the pH gradient would lower the system's efficiency. Moreover, a continuous feed of acid and base is expected to be a relevant cost factor. Therefore, bipolar water electrolyzer operation in pure water would be a more cost-efficient and sustainable scenario. Further, this configuration is expected to be more favorable for the AEM's durability as operation in strongly alkaline solutions is known to degrade the alkaline ionomers over time.[7] Thus, the high pH necessary to stabilize a PGM-free catalyst would rely on hydroxide supply through the AEM and AEI. Here, the hydroxide formation occurs through water dissociation at the bipolar interface (Fig. 1b).[23,28,29] Similarly, in an AEMWE operated in pure water, the OER catalyst would rely on the hydroxide generated in the HER (Fig. 1a).

In a recent study of our group on bipolar water electrolysis fed with pure water, we shifted the bipolar interface from the membrane center towards the anode. The aim was to reduce the impact of the poor AEM conductivity and potential water supply limitations toward the bipolar interface at higher current densities.[24] Hexamethyl-*p*-terphenyl poly(benzimidazolium) (HMT-PMBI, trade name Aemion) was employed as the AEM and a Nafion 212 membrane as the PEM. Like the findings for fuel cells,[17] the best performance was observed for an MEA where the bipolar interface was located directly between the AEI-based anode catalyst layer and the PEM without an additional AEM layer. This so-called *bipolar electrode membrane water electrolyzer* (*BPEMWE*) (Fig. 1c) was capable of exceeding the performance of a purely Nafion-based PEMWE reference under the same conditions, which was unexpected. The exact reasons for this circumstance could not be explained at that stage. It was assumed that the performance enhancement could be a combined effect of: (i) the large bipolar surface area enabled by the porous catalyst layer|membrane interface compared to a flat interface inside the membrane (Fig. 1b). (ii) Improved water management, as in the BPEMWE configuration, water only needed to be transported through the porous anode, whereas in the case of a BPMWE, water transport must occur additionally through the membrane. (iii) The assumption that IrO_2 works as a bifunctional catalyst for oxygen evolution (OER) and water dissociation (WD) into protons and hydroxide. It was possible to verify the water dissociation at the bipolar interface with an IrO_2 catalyst layer between AEM and PEM for an MEA design, as depicted in Fig. 1b. However, for the BPEMWE setup, neither a true pH gradient nor an actual

bipolar WD interface in the MEA could be proven by the methods applied in that work.

In this study, we investigate the BPEMWE system further to elucidate the reasons for improved performance compared to a PTE-based PEM electrolyzer. First, we use three-electrode measurements to analyze different ionomer thin films' effects on a Pt disk's surface pH as a high pH environment is indispensable for incorporating PGM-free catalyst materials. In the next step, we thoroughly evaluate the BPEMWE full cell performance characteristics with varying binder content to disentangle the reactions occurring at the bipolar interface and MEA design effects.

Materials and methods

Local pH measurement

Local pH measurements were conducted using a rotating disk electrode (RDE) setup with two polycrystalline Pt tips (*PINE Research*). One of the tips was coated with either a layer (~3 μm in dry state) of Nafion (D520, *Chemours*), high IEC Aemion, or Nafion on a layer of high IEC Aemion (Fig. S1†) to mimic the various ionomer environments occurring in a bipolar water electrolysis cell. The pH of ultrapure water, 0.1 M & 0.01 M $HClO_4$ (*Merck*, Suprapure), ultrapure water again, and 0.01 M & 0.1 M KOH (*Merck*, Emsure) was measured in this order and *vice versa* by determining the reversible hydrogen electrode (RHE) potential with the pure Pt tip.[30] Therefore, the electrolyte was purged with hydrogen, and the open circuit potential was determined after equilibrium was reached (Fig. S2 and S3†). To evaluate the impact of ionomer on the local pH at the catalyst, the ionomer-coated Pt tip was tested in each electrolyte subsequently. Between measurements, the ionomer-coated Pt tip was rinsed thoroughly and stored in ultrapure water. For the electrochemical measurements in a PTFE RDE cell, an Ag/AgCl reference electrode (*Metrohm*) was used.

MEA fabrication

All MEAs in this study were constructed employing catalyst coated porous transport electrodes (PTE) with an active area of 5 cm^2 and free-standing membranes of 16 cm^2. Nafion 115 and Nafion 211 (*Chemours*) served as the PEM, whereas 25 μm thick Aemion membranes (AF1-HNN8-25-X, *Ionomr Innovations Inc.*) were employed as AEM.

Nafion-based cathode electrodes ($cPTE_{ac}$) were fabricated by spraying a 1 wt% ink (2-propanol/water ratio 1 : 1) comprised of 20 wt% Nafion D520 (*Chemours*) and 80 wt% Pt/C catalyst (HiSPEC 9100, 60% Pt on Vulcan, *Johnson Matthey Fuel Cells*) on H24C5 (*Freudenberg*) gas diffusion layers (GDL) to a loading of 0.5 mg_{Pt} cm^{-2}.

For the anodes ($aPTE_{al}$ and $aPTE_{ac}$), titanium fiber sinter material (2GDL40-1.0, *Bekaert*) was coated with inks comprised of different amounts of the respective Aemion and Nafion (D520, *Chemours*) binders and IrO_2 (Premion, *Alfa Aesar*) to achieve an Ir loading of 1.5 mg cm^{-2}. It has to be noted that for the AEIs, materials with two different ion exchange capacities (IEC) were employed. For simplicity, we will refer to high IEC Aemion (IEC = 2.1–2.5 meq g^{-1}, AP1-HNN8-00-X), and low IEC Aemion (IEC = 1.4–1.7 meq g^{-1}, AP1-HNN5-00-X) in the following. All inks had a solid content of 1 wt%. Aemion based-inks were prepared in a 1 : 1 mixture of 1-propanol and water. In Nafion-based inks, 2-propanol was used as the ink alcohol in the same ratio.

Detailed fabrication parameters have been reported elsewhere.[24] Due to the prolonged precipitation of the IrO_2 nanoparticles, the binder content in the final catalyst layer is a multiple of the amount added to the ink in the first place. Therefore, the final binder content was determined *via* thermogravimetric analysis (TGA, STA 449 F1 Jupiter, *Netzsch*) with a heating rate of 10 K min^{-1} (30–600 °C), and rounded values are listed in Table 1.

For activation, Aemion membranes were immersed into 1 M KOH solution for 48 h and soaked in pure water for 12 h to remove residual KOH before cell assembly. All Aemion based electrodes were soaked in 1 M KOH solution for 12 h and rinsed thoroughly with deionized water before MEA construction. Nafion membranes were used as received.

Structural analysis

SEM structural analysis of the catalyst surface and morphology was carried out on quadratic 0.25 cm^2 spray-coated $aPTE_{al}$ with different high IEC Aemion binder contents according to Table 1. The samples were mounted on aluminum SEM specimen stubs with conductive and adhesive carbon tab. For better conductivity, the samples were carbon-coated (*Balzers Union*, MED 010). SEM imaging was performed with a Zeiss Crossbeam 540 focused ion beam scanning electron microscope (FIB-SEM) with a Gemini II column. All surface and cross-section SEM images were obtained with 3 kV accelerating voltage and a 750 pA beam current. For the cross-section images, a platinum layer was deposited *via* ion beam deposition using a gas injection system (*Orsay Physics*, MonoGIS) to shield the regions of interest from beam damage. Trenches were cut with an ion beam with an accelerating voltage of 30 kV and a current of 7 nA. The catalyst cross-section was polished successively with an ion beam of 30 kV and 700 pA, 30 kV acceleration voltage and 100 pA beam current.

Cell assembly and electrochemical characterization

MEA testing was carried out in a commercial electrolyzer cell test fixture (*Scribner Associates*) with single serpentine flow field geometry. For cell assembly, cathodes were placed onto the flow

Table 1 Overview of respective binder contents in the spray coating ink and the final catalyst layer determined from TGA measurements. This data applies for both low and high IEC and the 10 wt% Nafion catalyst layer

Binder content in ink solids [wt%]	Binder content in the final catalyst layer [wt%]
2	10
10	20
20	50

field in 180 μm tick PTFE frames (*HighTechFlon*). The membrane was added to the assembly before positioning the anode in its PTFE frame (1 mm thickness, *HighTechFlon*) on top and sealing the fixture with eight associated screws (tightening torque 8.5 N m).

Electrochemical characterization was carried out on a commercial test bench (600-ETS, *Scribner Associates*) equipped with an additional potentiostat (VSP-300, *BioLogic* with three additional 5 V/10 A booster boards). The anode was fed with an N_2-purged heated water flow of 40 mL min^{-1}, whereas the cathode was purged with 100 mL min^{-1} nitrogen at ambient pressure.

After heating the cell to the respective temperature (50 °C or 80 °C), a constant voltage of 1.8 V was applied to the cell for 1 h to equilibrate the system before the first polarization curve. For polarization curves, a series of galvanostatic electrochemical impedance spectroscopy (EIS) measurements were used to simultaneously determine the current dependent high-frequency resistance (HFR) from the *x*-intersection of the Nyquist plot. Each current step's hold time was 20 s with a subsequent mini EIS scan in the fashion of Suermann *et al.*[31] employing 10% of the direct current and acquiring 7 data points between 200 kHz to 1 Hz. After performance stabilization, the HFR-variation between individual polarization curves was <1 mΩ cm^2 in the current density range from 1–6 A cm^{-2}. To achieve a trade-off between sufficient resolution in the activation region and reasonable measurement time, the current step width was fixed to 1 mA cm^{-2} between 1–10 mA cm^{-2}, 10 mA cm^{-2} between 10–100 mA cm^{-2}, and 100 mA cm^{-2} between 100–6000 mA cm^{-2} or else the shut-off criterion of 2.3 V maximum cell voltage to prevent corrosion of the Ti parts. Due to the slightly different behavior of the individual MEAs, four polarization curves were recorded at 50 °C. Then the cell temperature was ramped to 80 °C, and after the constant-voltage period, polarization curves were recorded until the cell performance and the HFR remained constant between three individual measurements. Tafel slopes were determined by applying a linear fit between 10–100 mA cm^{-2} to the semi-logarithmic representation of the HFR-corrected polarization data. While the determined Tafel slopes at 50 °C exhibited errors in the range of ±2 mV dec^{-1}, the errors were found to be only in the range of ±1 mV dec^{-1} after performance stabilization at 80 °C.

The water quality was monitored using a built-in conductivity sensor (CDTX-11, *Omega*) and did not exceed 0.65 μS cm^{-1} at 80 °C in any measurement.

Results and discussion

Effect of ionomer binders on the local pH

To exploit one of the proposed main advantages in bipolar water electrolysis, the stable utilization of PGM-free catalysts at the anode, alkaline pH at the catalyst layer is indispensable.[32] Many literature reports on AEMWE,[10,33] and BPMWE[11,23] state that anion exchange ionomers can establish a high pH environment around the catalyst even under pure water operation.

To test this hypothesis, we aimed to clarify the pH conditions directly at the catalyst surface in contact with different ionomers under equilibrium conditions. Therefore, experiments on a model system using a polycrystalline Pt disk coated with thin layers of ionomer were performed to determine the pH from measuring the RHE potential (see materials and methods for further details).

Fig. 2a–c show that: (i) the fully humidified ionomer thin films do not significantly change the measured local pH at the Pt surface. Local pH rather follows the pH of the electrolyte. (ii) Some pre-history effects can be seen, especially when moving from an alkaline to a neutral environment. (iii) Even when immersed in ultrapure water, the ionomer coated samples do not significantly impact the local pH at the catalyst surface (Fig. 2d). The observed phenomena (i) and (iii) contradict the common assumption that a Nafion ionomer leads to a strongly acidic and anion exchange ionomers to an alkaline environment *per se*.

These observations suggest that in an electrolyzer system fully soaked in liquid water, the catalyst does most likely not experience any pH effect caused by the ionomer. As long as no electrical bias is applied, the catalyst in a water fed electrolyzer experiences a neutral pH environment independent of the type

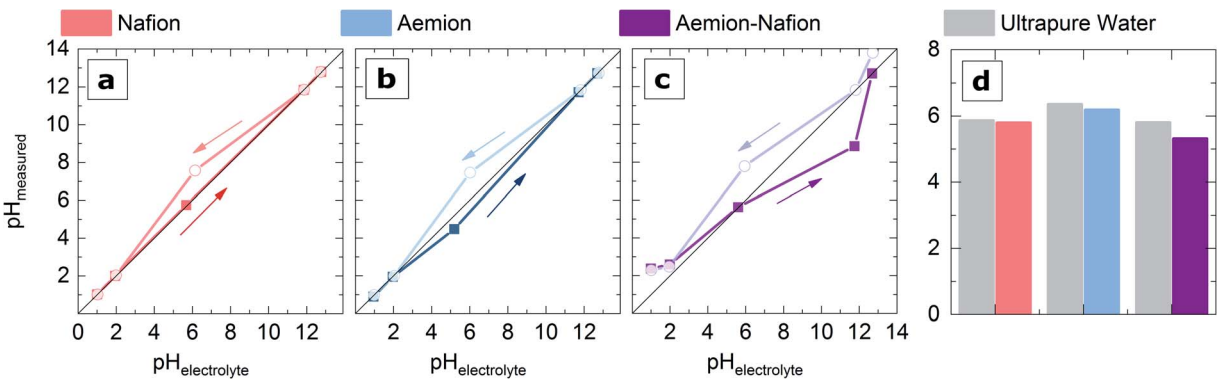

Fig. 2 Determination of the impact of different ionomers on the local pH at the electrode surface. (a–c) Comparison of local pH at ionomer coated polycrystalline Pt-disk in different electrolytes. (d) Results obtained in ultrapure water.

of polymer electrolyte. Consequently, the local pH in pure water fed MEAs during operation depends on the electrode reactions.

These findings could explain why so far – to the best of our knowledge – there is no literature report on a long-term stable AEMWE system operated in pure liquid water with platinum group metal (PGM) free catalysts.[34] According to Li *et al.*, the causes are twofold: The amount of alkaline functional groups (*e.g.*, ammonium groups) in state of the art AEMs is limited, and oxidation of phenyl groups in the polymer's backbone yields acidic phenol functionalities, which could partly neutralize the cationic fixed charges thus lowering the pH.[7] But perhaps the reasons are even more straightforward: Recently, Cao *et al.* were able to visualize hydroxide formation and conduction through a pH-indicator doped HMT-PMBI membrane. One crucial observation in this study was that at the anode, where alkaline OER (*i.e.*, hydroxide consumption to form O_2) occurs, the pH does not rise above 9.3, where the color change is expected for thymolphthalein.[35] It seems that hydroxide reaching the electrode is simultaneously consumed, and the local pH remains unclear. Also, for PEMWE systems, Knöppel *et al.* raised doubts about the *highly acidic* environment caused by the Nafion membrane supported by discrepancies in IrO_2 dissolution data for MEA- and *ex situ* catalyst investigations with externally defined pH.[36] For further investigations on the effect of AEI electrode binders in the BPEMWE setup and the role of the bipolar interface on the improved performance of this electrolyzer type, we used IrO_2 as the OER catalyst to exclude any potential effects of catalyst dissolution. An effect of the ionomer itself on the local pH in the MEA can be excluded from these observations.

Binder variation in BPEMWE MEA setup

We aimed to elucidate the reactions occurring at the anode|membrane interface in our BPEMWE MEAs (Fig. 1c) to understand the reasons for their improved performance compared to the PTE-based PEMWE reference. In our previous study, 10 wt% binder was used in the anode for both the PEMWE reference and the BPEMWE setups[24] because this was found to yield good performance and reproducibility for PEMWE MEAs.[37] A detailed study on the AEI binder content in the anode catalyst layer at constant catalyst loading was performed herein. Therefore, samples with 10, 20, and 50 wt% Aemion binder were prepared using the same spray-coating procedure.

Before evaluating the corresponding electrochemical performance data in detail, it is worth noting the catalyst layer structure for varying binder contents. The visible effects of increasing polymer contents were found to be comparable for Aemion and Nafion.[37] Therefore, only structures of the high IEC Aemion-based anodes are depicted in Fig. 3.

In the 10 wt% sample, binder and catalyst are evenly spread with a uniform pore size distribution (Fig. 3a). With increasing binder content, the porous structure becomes more and more inhomogeneous, exhibiting different domains (Fig. 3b and c). While the catalyst-rich part of the structure (bright areas) seems to be very similar to the overall catalyst layer of the 10 wt% sample, bulges of a polymer-rich phase (dark areas) protrude the porous layer. The share of these domains increases with increasing binder content. A similar phase separation phenomenon was also reported in the literature for increasing Nafion contents in spray-coated aPTEs for PEMWE. Poor cell performance due to high HFRs was the consequence.[37]

From these structures, different mechanistic scenarios for the reactions at the electrode|membrane interface can be expected, as summarized in Fig. 4. Scenario 1 – acidic OER reaction: considering a full MEA, large parts of the catalyst at the electrode surface directly contact the Nafion membrane for all samples. Consequently, simple acidic OER should be the locally predominant mechanistic scenario here. The protons generated are conducted through the PEM towards the cathode, just like in a regular PEMWE system (Fig. 4a).

Scenario 2 – bipolar interfacial reaction (Fig. 4b): the catalyst particles fully covered with AEI, particularly in the polymer-rich

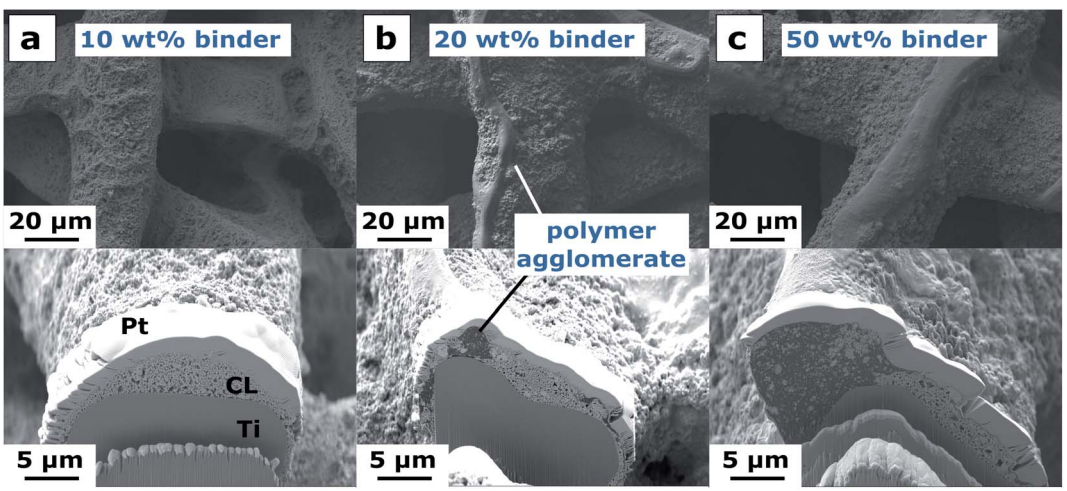

Fig. 3 Catalyst layer surface structure (top) and cross-section (bottom) for different binder contents of high IEC Aemion. Ir loading 1.5 mg cm^{-2}. (a) 10 wt%, (b) 20 wt%, (c) 50 wt% binder.

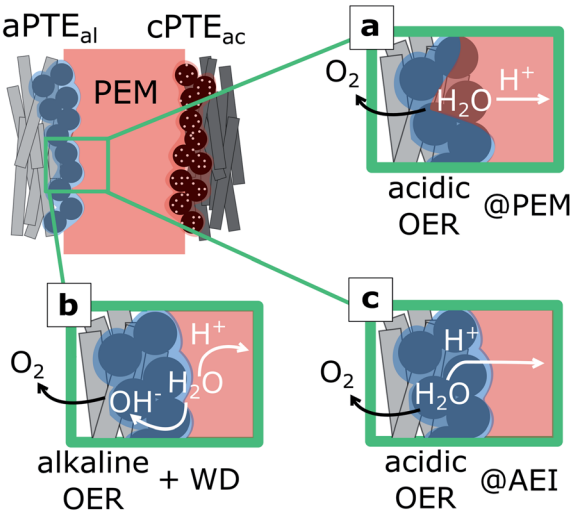

Fig. 4 Sketch of conceivable mechanistic scenarios at the electrode|membrane interface in BPEMWE. (a) IrO_2 in direct contact with Nafion membrane follows an acidic OER mechanism. (b) Bipolar interface in direct contact with IrO_2 catalyzes WD feeding alkaline OER mechanism. Protons are conducted through the PEM toward the cathode. (c) AEI solely acts as a binder and potentially dissipates protons from an acidic OER mechanism.

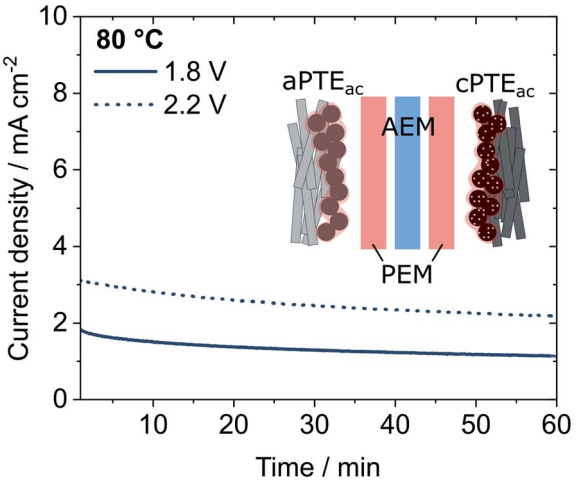

Fig. 5 Schematic and cell performance of a double-bipolar water electrolysis MEA. PEM-like conditions are established by aPTE$_{ac}$ and cPTE$_{ac}$ and two Nafion 211 membranes placed on the two sides of the 25 μm thick high IEC Aemion membrane. Constant voltage experiment.

domains, are most likely insulated from the Nafion membrane in a full MEA. Thus, in a genuinely bipolar case, water would be dissociated at the AEI|PEM interface. Protons would migrate towards the cathode through the PEM, while hydroxide is consumed in an alkaline OER reaction at the catalyst surrounded by the AEI. For this case, the permselectivity of the AEI is expected to be close to ideal. Scenario 3 – alkaline polymer only acts as binder: anticipating a finite proton conductivity of the AEI, it is also conceivable that the Aemion mainly acts as a binder in this system, and acidic OER is the predominant mechanism all over the catalyst layer, as depicted in Fig. 4c.

To analyze the influence of scenario 3 on the overall cell performance, a *double-bipolar* water electrolysis MEA was implemented, as depicted in Fig. 5. Catalyst layers ensured PEM-like OER and HER conditions for cathode and anode, as they were based on Nafion binders. Insulation of the 25 μm thick high IEC Aemion membrane from the catalyst was established by two additional 25 μm thick Nafion membranes placed on either side of the AEM. Consequently, the proton conductivity of the AEM is the performance determining factor in this electrolyzer setup. As the achieved current densities were extremely low, we consider the potential proton conductivity of the AEI in a pure-water fed electrolyzer and, therefore, scenario 3 (acidic OER in the AEI-rich domains) as negligible.

A well-known way to investigate anode kinetics in PEMWE research is Tafel analysis.[31] From a fundamental point of view, this method is valid when one reaction is significantly rate-determining. In a PEMWE MEA, the HER takes place on a Pt catalyst in a supposedly acidic environment. Its effect on the overall reaction rate is considered negligible,[38] which is also expected to be true for BPEMWE systems. The Tafel slope determined as a linear regression of a semi-logarithmic representation of the *iR*-corrected polarization data provides information about the anode kinetics.

However, for OER in acidic as well as in alkaline media, the mechanistic steps R_a3 and R_b3 (Table 2) are expected to be rate-determining and result in the same Tafel slope of 40 mV dec^{-1}.[39] Furthermore, considering the mechanistic picture drawn in Fig. 4b, it becomes apparent that the WD step postulated to happen at the AEI|PEM interface is equal to the R_a1 of the acidic OER mechanism. Assuming sufficient water supply, which is a prerequisite for both OER and WD, the two mechanisms depicted in Fig. 4 are indistinguishable from classical Tafel analysis only.

The performance of all MEAs in this study was investigated at cell temperatures of 50 °C and 80 °C. Fig. 6 features a summary of this data after break-in for the high IEC Aemion samples compared to a PEMWE reference in PTE-design.

Cell operation at 50 °C (Fig. 6c) revealed no significant difference in overall cell performance between the systems around moderate current density ranges (<1200 mA cm^{-2}). The 50 wt% binder sample has to be excluded from this comparison.

Table 2 Mechanistic steps of the oxygen evolution reaction (OER) under acidic and alkaline conditions. S represents an active catalyst site, and S–OH^{act} is an intermediate forming S–OH in the next step[39]

Water dissociation		
$H_2O \rightarrow H^+ + OH^-$		WD
Acidic OER mechanism	**Alkaline OER mechanism**	
$S + H_2O \rightarrow S\text{–}OH^{act} + H^+ + e^-$	$R_a1\ S + OH^- \rightarrow S\text{–}OH^{act} + e^-$	R_b1
$S\text{–}OH^{act} \rightarrow S\text{–}OH$	$R_a2\ S\text{–}OH^{act} \rightarrow S\text{–}OH$	R_b2
$S\text{–}OH \rightarrow S\text{–}O + H^+ + e^-$	$R_a3\ S\text{–}OH + OH^- \rightarrow S\text{–}O + H_2O + e^-$	R_b3
$S\text{–}O + S\text{–}O \rightarrow 2S + O_2$	$R_a4\ S\text{–}O + S\text{–}O \rightarrow 2S + O_2$	R_b4

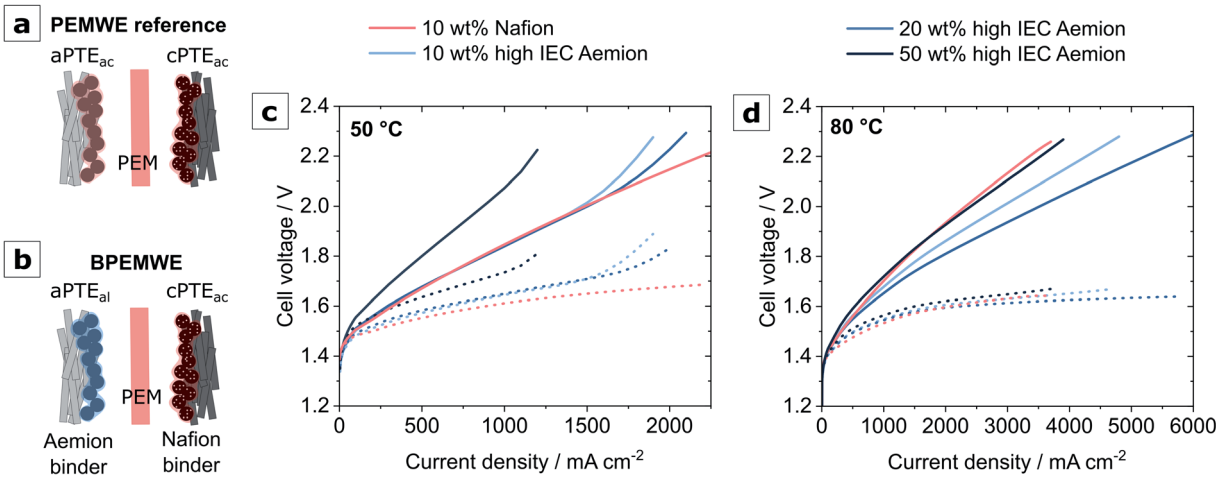

Fig. 6 Overview of MEA performance with varying binder types and binder contents in the anode electrode at constant Ir loading of 1.5 mg cm^{-2}. Schematic MEA structure for (a) PEMWE reference and (b) bipolar electrode|membrane interface water electrolyzer BPEMWE (c) Performance- and HFR-data at 50 °C cell temperature. (d) Performance- and HFR-data at 80 °C (dotted lines represent HFR-free cell voltage).

Its increased high-frequency resistance (HFR) and poor performance are expected for a sample with more than double the binder amount commonly found as the optimum in membrane-based electrolyzers.[38] The higher onset-potential at the lower operating temperature also suggests worse catalyst utilization compared to the other samples.

For high current densities, the polarization curves exhibited a shape commonly associated with mass transport overpotentials[40,41] were observed for the BPEMWE cells, which only improved slightly throughout the four polarization curves recorded at this cell temperature. The HFR-corrected polarization data reveals slightly superior kinetics of the PEMWE reference compared to the BPEMWE cells (Table 3). However, the BPEMWE MEAs compensate for their kinetic disadvantage with a lower HFR.

Significant differences in performance between the BPEMWE and the PEM reference were only observed when heating the cells to 80 °C. A comparison of performance after break-in is depicted in Fig. 6d. It becomes apparent that except for the 50 wt% sample, all BPEMWE MEAs exceeded the optimized[37] PEM reference performance.

An exciting feature is the noticeable break-in behavior of the BPEMWE cells. At an operating temperature of 50 °C, the overpotentials at high current densities attributed to mass transport limitations decreased to a shallow extent in subsequent polarization curves. However, when operating the system at 80 °C, the improvement between the individual polarization curves recorded is remarkable, exemplarily displayed for the 20 wt% high IEC Aemion sample in Fig. 7a. Throughout 10 polarization curves, this phenomenon vanished gradually until the cell performance remained stable. Even in a 100 h durability experiment, the HFR did not change anymore, as depicted in Fig. 7c.

In this study, all Aemion-based electrodes were preconditioned in 1 M KOH solution and deionized water under ambient conditions without additional degassing steps. Thus, particularly in the high IEC material, a significant amount of carbonates from the ambient air are expected to lower the material's hydroxide conductivity. It is known from fuel cell literature that these carbonates can be removed from the AEI when the devices are operated at high current densities.[42] We assume that precisely this phenomenon can be seen during the BPEMWE cells' break-in. No significant improvement is observed at

Table 3 Comparison of Tafel slopes at operating temperatures of 50 °C and 80 °C determined from polarization curves exhibiting stable cell performance (experimental error ~±2 mV dec^{-1} at 50 °C and ~±1 mV dec^{-1} at 80 °C) and relative performance improvement during break-in at 80 °C

		50 °C	80 °C	
Binder type in aPTE	Binder content [wt%]	Tafel slope [mV dec^{-1}]	Tafel slope [mV dec^{-1}]	Relative HFR improvement during break-in [%]
Nafion D520	10	44	42	2
High IEC Aemion	10	45	40	8
	20	49	40	15
	50	56	40	19
Low IEC Aemion	10	45	41	9
	20	48	41	10

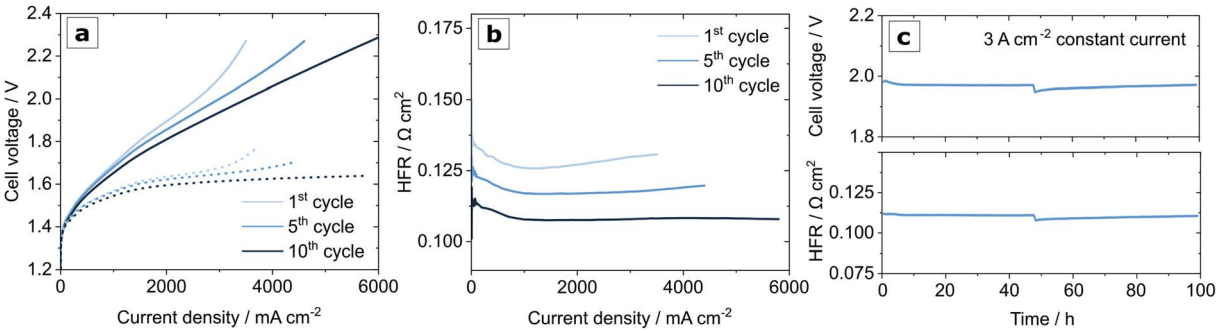

Fig. 7 Break-in behavior of BPEMWE MEA employing 20 wt% high IEC binder in the aPTE at 80 °C. (a) Selected polarization curves in the course of performance stabilization after the 10th cycle. Dotted lines represent the HFR-free data (b) associated HFR. (c) Durability test at 3 A cm^{-2} constant current for 100 h with a break for diagnostics after 50 h indicated by the spike in both cell voltage and HFR.

moderate currents (*e.g.*, cell operation at 50 °C or 1.8 V constant voltage hold before further characterization). The higher operating temperature enables operation at higher current densities, which favors the carbonate elimination from the AEI and gradually increases its hydroxide conductivity. A comparison of the relative HFR improvement during break-in at 80 °C is given in Table 3. For high IEC Aemion, the relative improvement is proportional to the catalyst layer's binder amount, supporting this hypothesis. Moreover, for Aemion with lower IEC, the improvement is less pronounced and does not change much with increasing binder content. With thinner Nafion 212 membranes allowing for much higher current densities as used in our previous study,[24] this break-in phenomenon could only be noticed in the first polarization curves as the carbonate was removed much faster under these conditions (Fig. S4†). While carbonates are removed from the ionomer, the hydroxide conductivity increases. Thus the IrO_2 inside the polymer-rich domains can be fed with hydroxide from water dissociation at the bipolar interface and becomes more and more active for alkaline OER.

For further evidence, a BPEMWE cell exhibiting stable performance and constant HFR at 80 °C was cooled down to an operating temperature of 50 °C without opening the nitrogen-purged electrolyzer system. Also, at the lower operating temperature, the pronounced overpotentials at high current densities were gone, and the HFR was drastically reduced compared to the polarization data acquired during the warm-up phase. Electrochemical impedance (EIS) analysis of the break-in behavior and associated polarization data can be found in Fig. S5.†

The break-in behavior serves as a strong indication for the existence of a water-splitting bipolar interface between the AEI based anode catalyst layer and the Nafion membrane in a BPEMWE MEA (scenario 2, Fig. 4b), whereas scenario 1 (Fig. 4a) cannot be excluded and is expected to happen simultaneously.

Reasons behind the improved performance

The findings above still do not fully explain the superior performance of the BPEMWE system as compared to the PEMWE reference at 80 °C. As the Tafel slopes after break-in are similar for both systems (Table 3) and no significant difference in onset-potentials is observed, the main difference is the drastically lower HFR. Further, in our previous study,[24] anodic PTEs containing 10 wt% low IEC Aemion were found to exceed the high IEC analogon's performance in the BPEMWE setup, which cannot straightforwardly be explained based on conductivity or swelling properties (see also Fig. S5†). The cell performance with varying binder content for low IEC Aemion based $aPTE_{al}$ was investigated to generate a better understanding, as depicted in Fig. 8. While the high IEC Aemion based BPEMWE systems drastically improved with increasing binder content, the performance for both the 10 wt% and the 20 wt% low IEC binder samples was the same within the expected error range, which is also true for their HFR. This finding implies that the low IEC binder's superior performance at low binder contents is somewhat based on structural reasons rather than on the polymer properties *per se*.

The SEM surface micrographs featured in Fig. 8c and d suggest that the formation of polymer-rich domains in the catalyst layer already happens for lower binder contents when low IEC Aemion is employed. As opposed to the findings for Nafion-based PTEs for PEMWE,[37] it seems that these substructures are favorable for the performance. The high IEC Aemion catalyst layer exhibits these polymer-rich substructures only for higher binder contents, as depicted in Fig. 3. However, as soon as these structures are available, the low IEC analogon's performance can be exceeded due to the higher conductivity of the high IEC samples.

The HFR represents the sum of ionic and electric resistances in the MEA, including the contact resistances between the individual layers.[31] Our study's findings suggest that BPEMWE features an alternative way of decreasing the contact resistance between the anode catalyst layer and membrane. Considering anion- and cation exchange polymers with fixed charges of opposite signs, ionic interactions can be expected to favor the adhesion between the two materials. This interaction appears to be more pronounced for the polymer-rich phases of the catalyst layer (Fig. 8e) and is improved with a high IEC as this quantity corresponds to the number of ionic groups in the polymer. This assumption is strongly supported by the visible adhesion of water-soaked Aemion and Nafion membranes as depicted in Fig. 8f and g and documented in a ESI Video.† It was observed that the two membranes could hardly be delaminated from

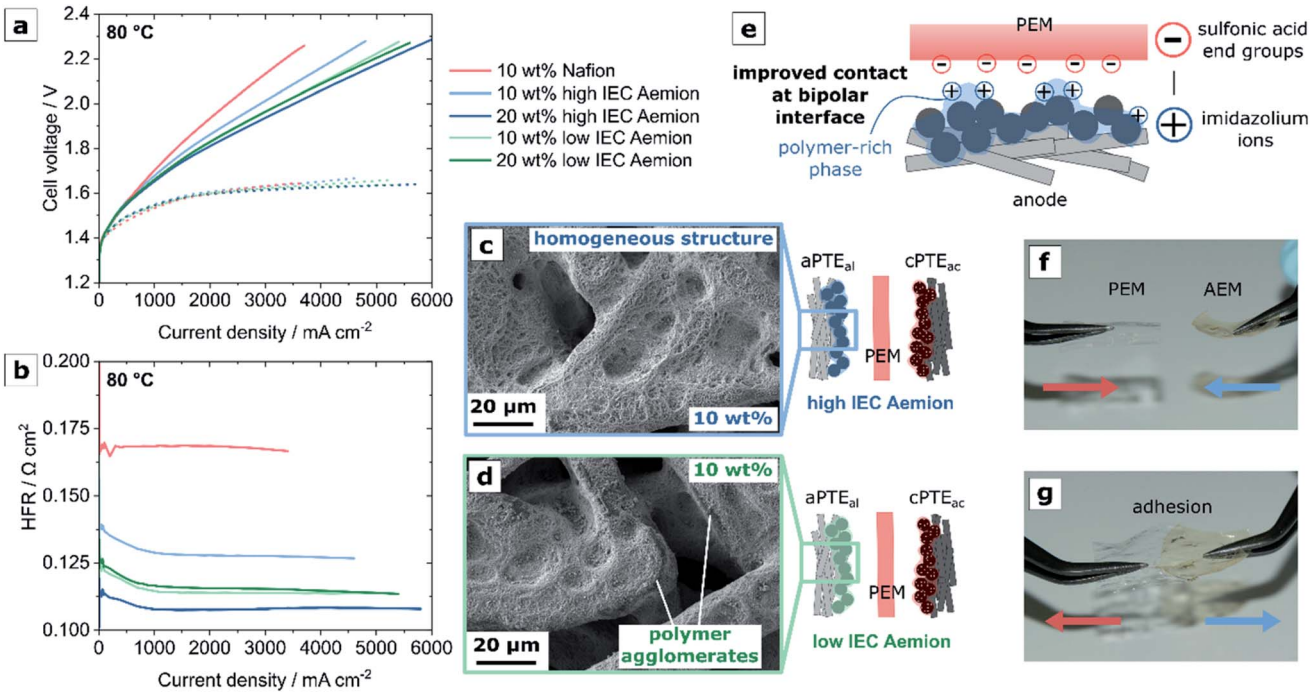

Fig. 8 (a) Performance data of BPEMWE (b) corresponding HFR. $aPTE_{al}$ IrO_2 catalyst layer structure with a binder content of 10 wt% for (c) high- and (d) low IEC Aemion. (e) Schematic of favored adhesion between AEI and PEM in polymer-rich phases of the catalyst layer as an effect of the polymer's fixed charges. (f) AEM and PEM after preconditioning soaked in pure water and (g) adhesion between membranes when bringing them into contact. See also ESI Video.†

each other once they had direct physical contact. It is more likely to break both membranes than removing the layers from each other. Further investigations are necessary to quantify the forces building up between the realistic layers.

It has to be noted that the HFR of the BPEMWE MEAs is lower than the PTE-based PEMWE reference but in a similar range as determined for an optimized catalyst coated membrane (CCM) PEMWE system. A comparison of performance and EIS data with a halfsided CCM as well as a PTE-based system with a non-conductive binder are summarized in Fig. S6 and S7.† In a CCM, the catalyst layer is directly applied to the membrane, *e.g.*, *via* decal transfer employing a hot-pressing step or other coating techniques employing liquid inks to establish good contact between these layers.[38] In a PTE-based system, hot-pressing of the porous transport electrode to the membrane is prone to membrane perforation and thus avoided. In the PTE-based MEA setup, it is impossible to exploit the critical feature of perfluorosulfonic acid polymers, their comparably low glass transition temperatures, which usually allow for facile material processing and low contact resistances. This drawback can be overcome using a bipolar approach.

Conclusion

We have shown that it is not possible to establish high- or low pH conditions at a metal surface only by applying thin films of anion- or cation exchange polymers, which could be the reason for the poor stability of PGM-free catalysts in pure water-fed AEMWE systems.[33] Moreover, local pH effects due to the ionomer itself cannot be held responsible for the different behavior of BPEMWE compared to PTE-based PEMWE.

A thorough investigation of BPEMWE full cell's break-in behavior combined with structural analysis of the anode catalyst layers served as a strong indication for the existence of a bipolar water splitting interface in this novel electrolyzer type. However, we found that the superior performance of BPEMWE compared to a PTE-based PEMWE reference is not caused by kinetic effects but rather by lower ohmic resistance in the MEA. As AEI-rich phases at the catalyst layer surface were found favorable for the cell performance and macroscopic adhesion between Aemion and Nafion membranes was observed even *ex situ*, we trace the reduced contact resistance in a BPEMWE system to ionic interactions at the interface between AEI and PEM.

From the findings of this study, we expect the adhesive forces between AEI binder and PEM to open new prospects for optimizing environmentally friendly hydrocarbon-based MEAs for water electrolysis mitigating the use of PFSAs.[43] Besides their potentially lower cost and reduced gas crossover, novel fluorine-free proton conducting polymers often exhibit the drawback of poor solubility in low-boiling alcohols, which are preferred ink-solvents as they are volatile and mostly less toxic. Further, their glass transition temperatures are commonly high, sometimes even exceeding their decomposition temperatures.[44] Ultimately, the production cost is an essential lever for the widespread application of a particular type of MEA. If the manufacturing of PTE-based systems should be more cost-efficient than that of

CCMs, the bipolar approach can optimize the ohmic losses in the electrolyzer.

Author contributions

B. M. prepared the MEA samples, performed electrochemical characterization and data analysis. Local pH measurements were conducted by K. E. with inputs from F. S. who recorded the supplementary video. Microstructural analysis was performed by M. B. and thermogravimetric analysis data was provided by J. B. The manuscript was written by B. M. with scientific input from all co-authors.

Conflicts of interest

The authors declare no competing financial interest.

Acknowledgements

This work was performed in collaboration with the National Research Council of Canada in the Materials for Clean Fuels Challenge Program. We want to acknowledge the helpful discussions with Dr Balázs Berkes, Dr Nadiia Kulyk, Dr Daniel Escalera, Dominik Seeberger, Adrian Hartert, and Anja Lončar on the local pH scenario. The authors would like to thank Dr Michel Suermann and Dr Thomas Böhm for their help with Tafel analysis and Anna Freiberg for discussions about MEA fabrication. Moreover, we are very thankful for the technical support provided by Achim Mannke, Stefan Borlein, and Stefan Fiegl.

References

1 K. Ayers, N. Danilovic, R. Ouimet, M. Carmo, B. Pivovar and M. Bornstein, Perspectives on Low-Temperature Electrolysis and Potential for Renewable Hydrogen at Scale, *Annu. Rev. Chem. Biomol. Eng.*, 2019, **10**, 219–239.

2 S. A. Grigoriev, V. N. Fateev, D. G. Bessarabov and P. Millet, Current status, research trends, and challenges in water electrolysis science and technology, *Int. J. Hydrogen Energy*, 2020, **45**(49), 26036–26058.

3 H. Lee, B. Lee, M. Byun and H. Lim, Economic and environmental analysis for PEM water electrolysis based on replacement moment and renewable electricity resources, *Energy Convers. Manage.*, 2020, **224**, 113477.

4 J. Brauns and T. Turek, Alkaline Water Electrolysis Powered by Renewable Energy: A Review, *Processes*, 2020, **8**, 248.

5 U. Babic, M. Suermann, F. N. Büchi, L. Gubler and T. J. Schmidt, Critical Review—Identifying Critical Gaps for Polymer Electrolyte Water Electrolysis Development, *J. Electrochem. Soc.*, 2017, **164**, F387–F399.

6 I. Vincent and D. Bessarabov, Low cost hydrogen production by anion exchange membrane electrolysis: A review, *Renewable Sustainable Energy Rev.*, 2018, **81**, 1690–1704.

7 D. Li, E. J. Park, W. Zhu, Q. Shi, Y. Zhou, H. Tian, Y. Lin, A. Serov, B. Zulevi, E. D. Baca, C. Fujimoto, H. T. Chung and Y. S. Kim, Highly quaternized polystyrene ionomers for high performance anion exchange membrane water electrolysers, *Nat. Energy*, 2020, **5**, 378–385.

8 I. Vincent, A. Kruger and D. Bessarabov, Development of efficient membrane electrode assembly for low cost hydrogen production by anion exchange membrane electrolysis, *Int. J. Hydrogen Energy*, 2017, **42**, 10752–10761.

9 Y. Leng, G. Chen, A. J. Mendoza, T. B. Tighe, M. A. Hickner and C.-Y. Wang, Solid-state water electrolysis with an alkaline membrane, *J. Am. Chem. Soc.*, 2012, **134**, 9054–9057.

10 J. R. Varcoe, P. Atanassov, D. R. Dekel, A. M. Herring, M. A. Hickner, P. A. Kohl, A. R. Kucernak, W. E. Mustain, K. Nijmeijer, K. Scott, T. Xu and L. Zhuang, Anion-exchange membranes in electrochemical energy systems, *Energy Environ. Sci.*, 2014, **7**, 3135–3191.

11 S. Z. Oener, S. Ardo and S. W. Boettcher, Ionic Processes in Water Electrolysis: The Role of Ion-Selective Membranes, *ACS Energy Lett.*, 2017, **2**, 2625–2634.

12 J. Luo, D. A. Vermaas, D. Bi, A. Hagfeldt, W. A. Smith and M. Grätzel, Bipolar Membrane-Assisted Solar Water Splitting in Optimal pH, *Adv. Energy Mater.*, 2016, **6**, 1600100.

13 Y. C. Li, Z. Yan, J. Hitt, R. Wycisk, P. N. Pintauro and T. E. Mallouk, Bipolar Membranes Inhibit Product Crossover in CO_2 Electrolysis Cells, *Adv. Sustainable Syst.*, 2018, **2**, 1700187.

14 A. Pătru, T. Binninger, B. Pribyl and T. J. Schmidt, Design Principles of Bipolar Electrochemical Co-Electrolysis Cells for Efficient Reduction of Carbon Dioxide from Gas Phase at Low Temperature, *J. Electrochem. Soc.*, 2019, **166**, F34–F43.

15 D. A. Salvatore, D. M. Weekes, J. He, K. E. Dettelbach, Y. C. Li, T. E. Mallouk and C. P. Berlinguette, Electrolysis of Gaseous CO_2 to CO in a Flow Cell with a Bipolar Membrane, *ACS Energy Lett.*, 2018, **3**, 149–154.

16 D. A. Vermaas and W. A. Smith, Synergistic Electrochemical CO_2 Reduction and Water Oxidation with a Bipolar Membrane, *ACS Energy Lett.*, 2016, **1**, 1143–1148.

17 M. Ünlü, J. Zhou and P. A. Kohl, Hybrid Anion and Proton Exchange Membrane Fuel Cells, *J. Phys. Chem. C*, 2009, **113**, 11416–11423.

18 Z. Wang, J. Parrondo, C. He, S. Sankarasubramanian and V. Ramani, Efficient pH-gradient-enabled microscale bipolar interfaces in direct borohydride fuel cells, *Nat. Energy*, 2019, **4**, 281–289.

19 D. Seeberger, D. McLaughlin, P. Hauenstein and S. Thiele, Bipolar-interface fuel cells – an underestimated membrane electrode assembly concept for PGM-free ORR catalysts, *Sustainable Energy Fuels*, 2020, **4**, 2508–2518.

20 J. Durst, C. Simon, A. Siebel, P. J. Rheinlander, T. Schuler, M. Hanzlik, J. Herranz, F. Hasche and H. A. Gasteiger, (Invited) Hydrogen Oxidation and Evolution Reaction (HOR/HER) on Pt Electrodes in Acid *vs.* Alkaline Electrolytes: Mechanism, Activity and Particle Size Effects, *ECS Trans.*, 2014, **64**, 1069–1080.

21 F. D. Speck, F. S. M. Ali, M. T. Y. Paul, R. K. Singh, T. Böhm, A. Hofer, O. Kasian, S. Thiele, J. Bachmann, D. R. Dekel, T. Kallio and S. Cherevko, Improved Hydrogen Oxidation Reaction Activity and Stability of Buried Metal-Oxide

Electrocatalyst Interfaces, *Chem. Mater.*, 2020, **32**, 7716–7724.

22 P. K. Giesbrecht, A. M. Müller, C. G. Read, S. Holdcroft, N. S. Lewis and M. S. Freund, Vapor-fed electrolysis of water using earth-abundant catalysts in Nafion or in bipolar Nafion/poly(benzimidazolium) membranes, *Sustainable Energy Fuels*, 2019, **3**, 3611–3626.

23 S. Z. Oener, M. J. Foster and S. W. Boettcher, Accelerating water dissociation in bipolar membranes and for electrocatalysis, *Science*, 2020, **369**(6507), 1099–1103.

24 B. Mayerhöfer, D. McLaughlin, T. Böhm, M. Hegelheimer, D. Seeberger and S. Thiele, Bipolar Membrane Electrode Assemblies for Water Electrolysis, *ACS Appl. Energy Mater.*, 2020, **3**(10), 9635–9644.

25 P. K. Giesbrecht and M. S. Freund, Recent Advances in Bipolar Membrane Design and Applications, *Chem. Mater.*, 2020, **32**(19), 8060–8090.

26 In *IUPAC Compendium of Chemical Terminology*, ed. M. Nič, J. Jirát, B. Košata, A. Jenkins and A. McNaught, IUPAC, Research Triangle Park, NC, 2009.

27 J. C. Bui, I. Digdaya, C. Xiang, A. T. Bell and A. Z. Weber, Understanding Multi-Ion Transport Mechanisms in Bipolar Membranes, *ACS Appl. Mater. Interfaces*, 2020, **12**(47), 52509–52526.

28 C. Shen, R. Wycisk and P. N. Pintauro, High performance electrospun bipolar membrane with a 3D junction, *Energy Environ. Sci.*, 2017, **10**, 1435–1442.

29 A. Hohenadel, D. Powers, R. Wycisk, M. Adamski, P. Pintauro and S. Holdcroft, Electrochemical Characterization of Hydrocarbon Bipolar Membranes with Varying Junction Morphology, *ACS Appl. Energy Mater.*, 2019, **2**(9), 6817–6824.

30 G. Jerkiewicz, Standard and Reversible Hydrogen Electrodes: Theory, Design, Operation, and Applications, *ACS Catal.*, 2020, **10**, 8409–8417.

31 M. Suermann, T. J. Schmidt and F. N. Büchi, Cell Performance Determining Parameters in High Pressure Water Electrolysis, *Electrochim. Acta*, 2016, **211**, 989–997.

32 M. Pourbaix, *Atlas of electrochemical equilibria in aqueous solutions*, National Association of Corrosion Engineers, Houston, Tex., 2nd edn, 1974.

33 M. Mandal, Recent Advancement on Anion Exchange Membranes for Fuel Cell and Water Electrolysis, *ChemElectroChem*, 2020, **8**, 36–45.

34 M. R. Kraglund, M. Carmo, G. Schiller, S. A. Ansar, D. Aili, E. Christensen and J. O. Jensen, Ion-solvating membranes as a new approach towards high rate alkaline electrolyzers, *Energy Environ. Sci.*, 2019, **12**, 3313–3318.

35 X. Cao, D. Novitski and S. Holdcroft, Visualization of Hydroxide Ion Formation upon Electrolytic Water Splitting in an Anion Exchange Membrane, *ACS Mater. Lett.*, 2019, **1**, 362–366.

36 J. Knöppel, M. Möckl, D. Escalera-López, K. Stojanovski, M. Bierling, T. Böhm, S. Thiele, M. Rzepka and S. Cherevko, *On the limitations in assessing stability of oxygen evolution catalysts using aqueous model electrochemical cells*, Research Square, 2020.

37 M. Bühler, F. Hegge, P. Holzapfel, M. Bierling, M. Suermann, S. Vierrath and S. Thiele, Optimization of anodic porous transport electrodes for proton exchange membrane water electrolyzers, *J. Mater. Chem. A*, 2019, **7**, 26984–26995.

38 M. Bernt and H. A. Gasteiger, Influence of Ionomer Content in IrO_2/TiO_2 Electrodes on PEM Water Electrolyzer Performance, *J. Electrochem. Soc.*, 2016, **163**, F3179–F3189.

39 Y. Zhao, N. M. Vargas-Barbosa, E. A. Hernandez-Pagan and T. E. Mallouk, Anodic deposition of colloidal iridium oxide thin films from hexahydroxyiridate(IV) solutions, *Small*, 2011, **7**, 2087–2093.

40 J. C. Garcia-Navarro, M. Schulze and K. A. Friedrich, Measuring and modeling mass transport losses in proton exchange membrane water electrolyzers using electrochemical impedance spectroscopy, *J. Power Sources*, 2019, **431**, 189–204.

41 E. T. Ojong, J. T. H. Kwan, A. Nouri-Khorasani, A. Bonakdarpour, D. P. Wilkinson and T. Smolinka, Development of an experimentally validated semi-empirical fully-coupled performance model of a PEM electrolysis cell with a 3-D structured porous transport layer, *Int. J. Hydrogen Energy*, 2017, **42**, 25831–25847.

42 U. Krewer, C. Weinzierl, N. Ziv and D. R. Dekel, Impact of carbonation processes in anion exchange membrane fuel cells, *Electrochim. Acta*, 2018, **263**, 433–446.

43 R. Lohmann, I. T. Cousins, J. C. DeWitt, J. Glüge, G. Goldenman, D. Herzke, A. B. Lindstrom, M. F. Miller, C. A. Ng, S. Patton, M. Scheringer, X. Trier and Z. Wang, Are Fluoropolymers Really of Low Concern for Human and Environmental Health and Separate from Other PFAS?, *Environ. Sci. Technol.*, 2020, **54**, 12820–12828.

44 M. Adamski, T. J. G. Skalski, B. Britton, T. J. Peckham, L. Metzler and S. Holdcroft, Highly Stable, Low Gas Crossover, Proton-Conducting Phenylated Polyphenylenes, *Angew. Chem., Int. Ed.*, 2017, **56**, 9058–9061.